Fractal scattering dynamics of the three-dimensional HOCl molecule

Yi-Der Lin, Alex M. Barr, and L. E. Reichl
Center for Complex Quantum Systems and Department of Physics The University of Texas at Austin, Austin, Texas 78712, USA

Christof Jung
Instituto de Ciencias Fisicas, Universidad Nacional Autonoma de Mexico Av. Universidad 1001, 62251 Cuernavaca, Mexico
(Received 30 May 2012; published 30 January 2013)

We compare the 2D and 3D classical fractal scattering dynamics of Cl and HO for energies just above dissociation of the HOCl molecule, using a realistic potential energy surface for the HOCl molecule and techniques developed to analyze 3D chaotic scattering processes. For parameter regimes where the HO dimer initially has small vibrational energy, only small intervals of initial conditions show fractal scattering behavior and the scattering process is well described by a 2D model. For parameter regimes where the HO dimer initially has large vibrational energy, the scattering process is fully 3D and is dominated by fractal behavior.

DOI: 10.1103/PhysRevE.87.012917 PACS number(s): 05.45.Ac, 34.20.−b, 34.50.Ez

I. INTRODUCTION

Studies of fractal scattering processes have focused on systems with two degrees of freedom (2D) because in 2D they are easy to visualize [1–8] and characterize using Poincaré surfaces of section (SOS). In 2D systems it is possible to follow the flow of stable and unstable manifolds, as they form an increasingly complex network of tendrils in the phase space. These tendrils can be categorized in terms of symbolic dynamics and their fractal structure then becomes apparent.

When dealing with scattering problems with three degrees of freedom (3D), surfaces of section (SOS) become four dimensional and one cannot visualize the complexity of the scattering processes in the same way [9], although the scattering process is still dominated by the normal hyperbolic invariant manifold (NHIM) of the outer fixed point of the SOS. Jung *et al.* [10] have shown that in some parameter regimes, a 3D system can be viewed as a 2D system with a weakly coupled third degree of freedom for which an approximate conserved quantity (exact for the 2D system) exists. The four-dimensional surface of section can then be viewed as a continuous "stack" of two-dimensional surfaces of section. The outer fixed point of the "stack" of 2D systems forms a continuous NHIM [9,11–13]. They find that this NHIM and its homoclinic tangle appear to remain structurally robust in the presence of a small perturbation.

In subsequent sections, we analyze the scattering dynamics of Cl and HO just above the dissociation energy of the HOCl molecule. Our analysis of Cl-HO scattering dynamics uses a potential energy surface (PES), constructed by Weiss *et al.* [14,15], that realistically governs the dynamics of the bound HOCl molecule and the Cl-HO scattering system for an interval of energies just above dissociation of Cl from HO. For the 3D Cl-HO scattering process, we find behavior similar to that observed by Jung *et al.* [10], with the vibrational degree of freedom of HO playing the role of a weakly coupled third degree of freedom (at least for some parameter regimes). For a given initial energy of Cl and HO, the initial conditions of both objects can be specified in terms of two initial "phases" (which we define below). Evidence of the robustness of the NHIM in the Cl-HO system can be seen in plots of the magnitude of the outgoing momentum of the scattered Cl atom as a function of the initial phases. This provides a "landscape" that shows a range of initial phases for which the scattering function (outgoing momentum versus initial phases) appears to have fractal structure. This fractal structure is formed by the intersection of the stable manifold of the NHIM (which extends into the asymptotic region) with the torus formed by the initial phases of Cl and HO in the asymptotic region. When a Cl trajectory has an initial phase that lies on the NHIM in the asymptotic region, the subsequent trajectory of Cl will have an infinite delay time and the outgoing Cl momentum will approach zero in the asymptotic region as the trajectory approaches the outer fixed point (which by definition has zero momentum). These singular points form a fractal structure which is an intrinsic property of the molecule, and all other dynamical quantities will exhibit this same fractal behavior.

We begin in Sec. II with a description of the Hamiltonian and the potential energy surface for the 3D HOCl molecule. In Sec. III, we describe the scattering dynamics. In Sec. IV, we compare the scattering dynamics of the 3D and 2D models of the HOCl molecule for the case when the HO dimer initially has a small amount of vibrational energy. In Sec. V, we show the effect on the scattering phase space of starting the scattering process with the HO dimer in a fairly high energy vibrational state. In Sec. VI, we make some concluding remarks.

II. THE 3D MODEL OF HOCL

In its bound configuration, the HOCl molecule consists of H, O, and Cl atoms, with masses m_H, m_O, and m_{Cl}, respectively. The molecule dissociates into a free Cl atom and a bound HO molecule above $E = 20\,312\ \mathrm{cm}^{-1}$. The classical dynamics of the HOCl system has been discussed in Ref. [7] for a 2D version of the molecule in which the HO bond is held fixed. We here relax that constraint on the HO bond and consider the 3D dynamics of the molecule. As in Ref. [7], we introduce laboratory coordinates (x',y',z') and body-fixed coordinates (x,y,z) whose origin is the center of mass of the molecule. The total angular momentum of the molecule, $\mathbf{L}_{\mathrm{tot}}$, is conserved. We assume that all of the dynamics occurs in the (x',z') and (x,z) planes and that any angular momentum vectors generated by internal rotations of the molecule lie along parallel y' and

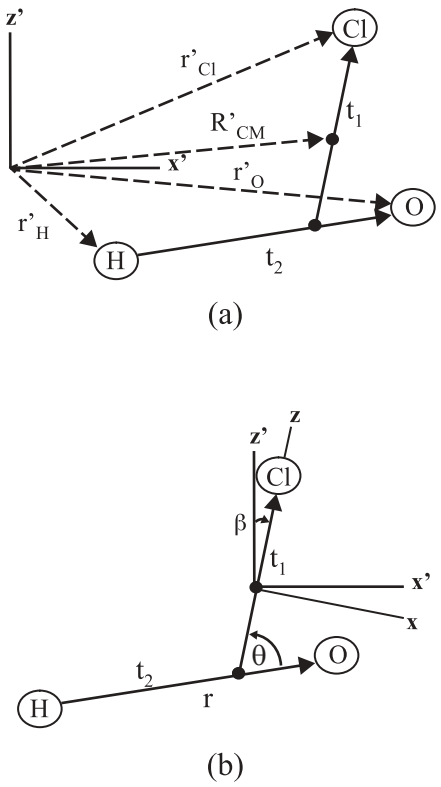

FIG. 1. (a) Relationship between laboratory frame coordinates and Jacobi vectors $\mathbf{t}_1$ and $\mathbf{t}_2$ and θ. (b) Body-fixed and laboratory axes differ by the angle β so $\mathbf{t}_1$ always lies along the body z axis.

y axes in the laboratory and body-fixed frames, respectively. A sketch of HOCl relative to the laboratory and body frames is shown in Fig. 1.

Let $\mathbf{t}_1$ be a vector of length R that connects the center of mass of HO to Cl and $\mathbf{t}_2$ a vector of length r that connects H to O. The angle between $\mathbf{t}_1$ and $\mathbf{t}_2$ is θ where $\theta = 0$ for the linear configuration H-O-Cl. The center of mass of the molecule lies along $\mathbf{t}_1$ a distance $m_d R/M$ from the Cl atom, where $m_d = m_{\rm O} + m_{\rm H}$ and $M = m_{\rm Cl} + m_{\rm O} + m_{\rm H}$. Let $\mathbf{r}'_{\rm Cl}$, $\mathbf{r}'_{\rm H}$, and $\mathbf{r}'_{\rm O}$ denote the displacement of the Cl, H, and O atoms from the laboratory frame origin. Let $\mathbf{R}_{\rm c.m.} = (m_{\rm Cl}\mathbf{r}'_{\rm Cl} + m_{\rm O}\mathbf{r}'_{\rm O} + m_{\rm H}\mathbf{r}'_{\rm H})/M$ denote the displacement of the center of mass of HOCl from the laboratory frame origin. The kinetic energy then is given by

$$T = \frac{M}{2}\dot{\mathbf{R}}^2_{\rm c.m.} + \frac{\mu_1}{2}\dot{\mathbf{t}}_1^2 + \frac{\mu_2}{2}\dot{\mathbf{t}}_2^2 \tag{1}$$

and the total angular momentum is given by

$$\mathbf{L}_{\rm tot} = \mu_1 \mathbf{t}_1 \times \dot{\mathbf{t}}_1 + \mu_2 \mathbf{t}_2 \times \dot{\mathbf{t}}_2, \tag{2}$$

where $\mu_1 = \frac{m_{\rm Cl} m_d}{M} = \frac{595}{52}u$ and $\mu_2 = \frac{m_{\rm H} m_{\rm O}}{m_d} = \frac{16}{17}u$ (u the atomic mass unit).

We will assume that $\mathbf{t}_1$ lies along the body z axis and that the body y axis is directed perpendicularly to the plane of the molecule. We can then write $\mathbf{t}_1 = R\hat{\mathbf{z}}$ and $\mathbf{t}_2 = r\sin(\theta)\hat{\mathbf{x}} + r\cos(\theta)\hat{\mathbf{z}}$. We further assume that the body frame (x,z) axes make an angle β with respect to the laboratory frame (x',z') axes so if the two frames rotate relative to one another, the angular velocity of rotation is $\dot{\beta}\hat{\mathbf{y}}$.

The Hamiltonian for the HO + Cl system (dropping the center-of-mass motion) can then be written in the form

$$H = \frac{p_R^2}{2\mu_1} + \frac{p_r^2}{2\mu_2} + \frac{p_\theta^2}{2\mu_2 r^2} + \frac{p_\theta^2}{2\mu_1 R^2} + \frac{p_\beta^2}{2\mu_1 R^2} - \frac{p_\theta p_\beta}{\mu R^2} + D_e V(R,\theta,r) = E, \tag{3}$$

where E is the total energy. The quantity $D_e V(R,\theta,r)$ is the potential energy and $D_e = 20\,312.3\ {\rm cm}^{-1} = 2.518$ eV is the energy at which Cl dissociates from HO. The canonical momenta p_R, p_r, p_θ, and p_β can be written $p_R = \mu_1 \dot{R}$, $p_r = \mu_2 \dot{r}$, $p_\theta = \mu_2 r^2(\dot{\theta} + \dot{\beta})$, and $p_\beta = \mu_2 r^2(\dot{\theta} + \dot{\beta}) + \mu_1 R^2 \dot{\beta}$. The total angular momentum of the molecule is then given by

$$\mathbf{L}_{\rm tot} = \mathbf{L}_1 + \mathbf{L}_2 = p_\beta \hat{\mathbf{y}}, \tag{4}$$

where

$$\begin{aligned} \mathbf{L}_1 &= \mu_1 \mathbf{t}_1 \times \dot{\mathbf{t}}_1 = \mu_1 R^2 \dot{\beta}\hat{\mathbf{y}} \text{ and} \\ \mathbf{L}_2 &= \mu_2 \mathbf{t}_2 \times \dot{\mathbf{t}}_2 = \mu_2 r^2(\dot{\theta} + \dot{\beta})\hat{\mathbf{y}}. \end{aligned} \tag{5}$$

In subsequent sections, we shall examine the scattering of Cl from HO for a subset of initial conditions for which $\mathbf{L}_{\rm tot} = 0$. We accomplish this by requiring that $p_\beta = 0$ in all initial trajectories. Since total angular momentum is conserved for the HOCl system, then $p_\beta = 0$ for the entire scattering process. Note, however, that $\mathbf{L}_1$ and $\mathbf{L}_2$ need not be zero so Cl and HO can rotate relative to one another.

It is useful to write the above quantities in terms of dimensionless units (d.u.). We parametrize all energies in units of D_e, lengths in units of the Bohr radius $a_B = 5.2917 \times 10^{-11}$ m, and angular momenta in terms of Planck's constant $\hbar = 1.05457 \times 10^{-34}$ J s. Then $H = D_e H'$, $E = D_e E'$, $R = a_B R'$, $r = a_B r'$, $p_R = \frac{\hbar}{a_B} p'_R$, $p_r = \frac{\hbar}{a_B} p'_r$, $p_\theta = \hbar p'_\theta$, $p_\beta = \hbar p'_\beta$, and time $t = \frac{\hbar}{D_e} t'$, where primed quantities are dimensionless. If we now drop the primes on dimensionless quantities, the (dimensionless) Hamiltonian takes the form

$$H = \frac{p_R^2}{2\delta_1} + \frac{p_r^2}{2\delta_2} + \frac{p_\theta^2}{2\delta_2 r^2} + \frac{p_\theta^2}{2\delta_1 R^2} + \frac{p_\beta^2}{2\delta_1 R^2} - \frac{p_\theta p_\beta}{\delta_1 R^2} + V(R,\theta,r) = E, \tag{6}$$

where $\delta_1 = \frac{\mu_1 D_e a_B^2}{\hbar^2} = 1930.3$ d.u. and $\delta_2 = \frac{\mu_2 D_e a_B^2}{\hbar^2} = 158.79$ d.u. Since we are considering scattering dynamics for the case $p_\beta = 0$, this reduces to a system with three degrees of freedom.

We use the potential energy surface (PES) constructed by Weiss *et al.* [14,15] which governs the dynamics of the HOCl molecule and the Cl and HO system for a region of energies just above dissociation of Cl from HO. This PES can be written in the form

$$V(R_{\rm OCl}, R_{\rm HO}, R_{\rm ClH}) = V_I(R_{\rm OCl}, R_{\rm HO}, R_{\rm ClH}) + V_{\rm HO}(R_{\rm HO}). \tag{7}$$

where $R_{\rm OCl}, R_{\rm HO}$, and $R_{\rm ClH}$ are the distances between O and Cl, H and O, and Cl and H, respectively (in dimensionless

units), and

$$V_{\rm HO}(R_{\rm HO}) = 1.835[1 - e^{-\beta_{\rm HO}(R_{\rm HO}-\bar{R}_{\rm HO})}]^2, \quad (8)$$

is the potential energy of the HO system in the asymptotic region with $\beta_{\rm HO} = 1.2139$ d.u. and $\bar{R}_{\rm HO} = 1.8323$ d.u. The potential energy $V_I(R_{\rm OCl}, R_{\rm HO}, R_{\rm ClH})$ is the interaction energy of Cl and HO and has the form

$$V_I(R_{\rm OCl}, R_{\rm HO}, R_{\rm ClH}) = \frac{1}{2}[1 + \tanh(6 - R_{\rm ClO})] \times \sum_{i=0}^{7}\sum_{j=0}^{7}\sum_{\ell=0}^{7} a_{i,j,\ell} g_i(R_{\rm HO}) h_j(R_{\rm OCl}) d_\ell(R_{\rm ClH}), \quad (9)$$

where

$$g_i(R_{\rm HO}) = [1 - e^{-k_{\rm HO}(R_{\rm HO}-\bar{R}_{\rm HO})}]^i,$$
$$h_j(R_{\rm OCl}) = [1 - e^{-k_{\rm OCl}(R_{\rm OCl}-\bar{R}_{\rm OCl})}]^{j+1}, \quad (10)$$
$$d_\ell(R_{\rm ClH}) = [1 - e^{-k_{\rm ClH}(R_{\rm ClH}-\bar{R}_{\rm ClH})}]^\ell,$$

$\bar{R}_{\rm HO} = 1.85$ d.u., $\bar{R}_{\rm OCl} = 3.2$ d.u., $\bar{R}_{\rm ClH} = 4$ d.u., $k_{\rm HO} = 0.3$ d.u., $k_{\rm OCl} = 0.8$ d.u., and $k_{\rm ClH} = 0.1$ d.u. Note that $R_{\rm HO} = r$ and the distances $R_{\rm OCl}$, $R_{\rm HO}$, and $R_{\rm ClH}$ are related to R, r, and θ by the triangle equations

$$R_{\rm OCl} = \sqrt{\left(\frac{m_H}{m_d}\right)^2 r^2 + R^2 - 2\left(\frac{m_H}{m_d}\right) r R\cos(\theta)} \quad (11)$$

and

$$R_{\rm ClH} = \sqrt{\left(\frac{m_O}{m_d}\right)^2 r^2 + R^2 + 2\left(\frac{m_O}{m_d}\right) r R\cos(\theta)}. \quad (12)$$

The ground-state (lowest bound state) energy for this system is $E = 0$ d.u. The dissociation energy for Cl from HO, when rotation and vibration energy of HO is zero, is $E = D_e = 1.0$ d.u. The 2D model of HOCl is obtained by setting $r = \bar{R}_{\rm HO}$ and $p_r = 0$ in Eq. (6) and $R_{\rm HO} = \bar{R}_{\rm HO}$ in Eqs. (8) and (10).

III. SCATTERING DYNAMICS

In the 3D model of HOCl, the energy and the total angular momentum of the HOCl system are constants of the motion, and both the HO rotation and vibration participate in the dynamics of the scattering process. For energies just above dissociation, Cl impinges on the HO complex and scatters from it, leaving both the Cl atom and the HO complex in an altered state. In order to study this scattering process, we must specify initial conditions for both the Cl atom and the HO complex.

We can distribute the initial total energy E (which is conserved) between the incident energy of Cl, $E_{\rm Cl} = \frac{p_R^2}{2\delta_1}$, and the rotational and vibration energies of HO, $E_{\rm rot}$ and $E_{\rm vib}$, so $E = E_{\rm Cl} + E_{\rm rot} + E_{\rm vib}$. The initial value of $E_{\rm Cl}$ fixes the initial value of p_R. The remaining energy is distributed between $E_{\rm rot}$ and $E_{\rm vib}$. The angular momentum of HO relative to its center of mass is given by $\mathbf{L}_2 = p_\theta \hat{\mathbf{y}}$. For a given total energy E, in the asymptotic region ($R_{\rm in} = R_{\rm out} = 12$ d.u.), we can specify a range of initial values of $E_{\rm Cl}$. We also specify a range of initial values for the angular position $\chi = \theta$ and vibrational phase ψ in the asymptotic region. Each initial condition therefore can be labeled uniquely by $(E, p_R, p_\theta, \chi, \psi)$.

The phase $\chi = \theta$ is the initial angular position of the HO dimer at $R_{\rm in} = 12$ d.u. The phase ψ is determined by the initial vibrational configuration of HO in the asymptotic region and ranges over all possible initial configurations of HO at its given initial energy. It is determined as follows. In the asymptotic regime the Hamiltonian of HO is given by

$$H_{\rm HO} = \frac{p_r^2}{2\delta_2} + \frac{p_\theta^2}{2\delta_2 r^2} + V_{\rm HO}(r) = E_{\rm rot} + E_{\rm vib} = E_{\rm HO}. \quad (13)$$

The value of p_θ and the total energy of HO are fixed, and the initial values of (p_r, r) are allowed to range over one complete oscillation of the HO vibration at that total energy. The phase ψ ranges over the interval $0 \leqslant \psi \leqslant 2\pi$ as HO goes through one complete oscillation.

For a given value of total energy E, we can plot values of p_R and p_θ after the scattering process has occurred for ranges of initial phases $0 \leqslant \chi \leqslant 2\pi$ and $0 \leqslant \psi \leqslant 2\pi$ and different incident Cl energies $E_{\rm Cl}$. In subsequent sections, we analyze scattering properties for a subspace of the scattering process with total angular momentum zero and total energies in the interval 1.034 d.u. $\leqslant E \leqslant$ 1.231 d.u. (21 000 cm$^{-1} \leqslant E \leqslant$ 25 000 cm^{-1}). The PES that we use was developed to represent the dynamics of HOCl above dissociation for these and slightly higher energies. The subspace with total angular momentum zero gives us a good picture of the nature of the scattering processes. We do not expect it to change significantly for nonzero total angular momentum.

In the scattering process, the total energy is distributed between the rotational and vibrational energy of HO and the incident energy of Cl in different ways. If Cl approaches HO with its momentum directed along a line through the center of mass of HO, then its impact parameter is zero and HO does not rotate. If Cl approaches HO with a nonzero impact parameter relative to the center of mass of HO, then it will have angular momentum and the HO molecule will rotate in such a manner that its rotational angular momentum cancels the angular momentum of the Cl atom. In the energy interval 1.034 d.u. $\leqslant E \leqslant$ 1.231 d.u., HO remains a bound molecule and acts dynamically like an anharmonic oscillator that is coupled into the scattering between the center of mass of HO and the Cl atom.

IV. 2D VERSUS 3D MODELS OF HOCl

The HO vibration is very stiff compared to that of the HO-Cl vibration. This fact has formed the basis of two papers that have modeled the dynamic properties of the HOCl molecule as a 2D system, holding the HO vibration fixed [7,16]. In this and subsequent sections, we compare the scattering dynamics of the 2D and 3D models of HOCl at energies above dissociation.

In Fig. 2, we compare the scattering behavior of p_R and p_θ for the 3D case, when the total energy of the Cl + HO system is $E = 1.231$ d.u. $= 25\,000$ cm^{-1}, the HO molecule has an initial total energy $E_{\rm HO} = 0.03282$ d.u. $= 667$ cm^{-1}, and an initial angular momentum $p_\theta = 5.92$ d.u. For these parameters, the initial energy of HO is almost entirely rotational. The initial range of oscillation of HO is 1.8333 d.u. $\leqslant r \leqslant$ 1.8446 d.u.,

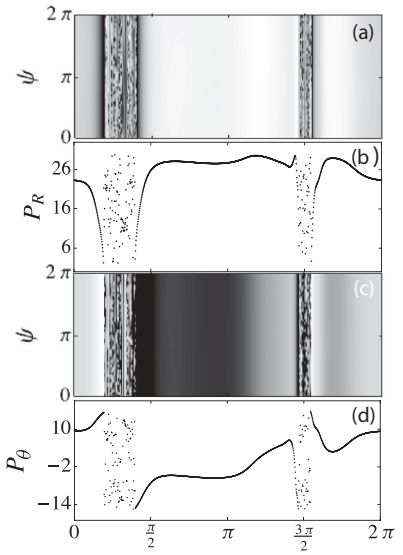

FIG. 2. The scattering dynamics for the 3D molecule when total energy of the Cl + H-O system is $E = 1.231$ d.u. $= 25\,000$ cm^{-1}. The HO dimer has an initial total energy $E_{\rm HO} = 0.03261.231$ d.u. $=$ 667 cm^{-1}. The initial value of p_θ is $p_\theta = 5.92$ d.u. With this value of p_θ, HO is essentially in its vibrational ground state initially. (a) A contour plot of scattered values of p_R as a function of ψ (vertical axis) and χ (horizontal axis). (b) A plot of scattered values of p_R as a function of χ for $\psi = \pi$. Intervals of continuity and chaos are clearly seen. (c) A contour plot of scattered values of p_θ as a function of ψ (vertical axis) and χ (horizontal axis). (d) A plot of scattered values of p_θ as a function of χ for $\psi = \pi$. The intervals of continuity and of discontinuity are the same as those of p_R, indicating that they are an intrinsic property of the molecule. All plots contain 1000 data points along the χ axis and 50 data points along the ψ axis. The grayscale in (a) and (c) ranges from 0 to 32, with 32 the lightest shade. Values of p_R and p_θ at the darkest and lightest points in (a) and (c) can be read from (b) and (d), respectively. (p_R and p_θ in dimensionless units and χ and ψ in radians.)

so HO is close to its minimum vibration energy. Figures 2(a) and 2(c) show contour plots of scattered values of p_R and p_θ, respectively, as a function of ψ (vertical axis) and χ (horizontal axis). Figures 2(b) and 2(d) show plots of scattered values of p_R and p_θ, respectively, as a function of χ for fixed $\psi = \pi$ (for $\psi = \pi$, HO is initially at the turning point with minimum value of r). All of the plots in Fig. 2 contain 1000 data points for χ and 50 data points for ψ. Figures 2(b) and 2(d) show that the scattering data contain large ranges of χ with intervals of continuity and two shorter ranges of χ that contain a fractal distribution (of measure zero) of singularities. These are actually points of intersection of the stable manifold of the outer NHIM with the set of initial conditions. The fractal set of singularities form the boundaries of a complimentary fractal set of intervals of continuity, so the scattering function becomes discontinuous in this region. In Fig. 2, these intervals of continuity and singular points appear to be approximately independent of ψ (the initial configuration of HO). This indicates that the scattering dynamics is well approximated by the 2D model used in Refs. [7,16] in which the HO vibration is held fixed. The fractal nature of the scattering process is intrinsic to the Cl-HO system above dissociation and the same

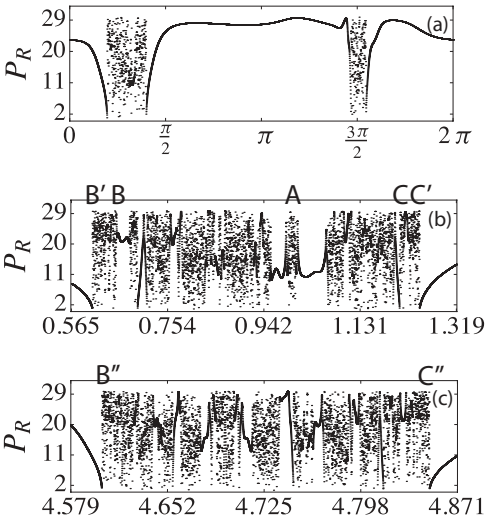

FIG. 3. Scattering dynamics of the 3D Cl-HO system. (a) Magnification of Fig. 2(b) (5000 data points for χ). (b) Magnification of the left discontinuous region of Fig. 3(a). (c) Magnification of the right discontinuous region of Fig. 3(a). (p_R in dimensionless units and χ in radians.)

fractal structure will appear in all scattering functions. This can be seen in the Figs. 2(a) and 2(c), which show asymptotic values of p_R and p_θ after the scattering process. The fractal structure of these plots is identical.

In Fig. 3(a), we again plot p_R versus χ, as in Fig. 2(b), but now with 5000 data points for χ, so more of the fractal structure emerges. In Figs. 3(b) and 3(c), we enlarge the fractal regions on the left and right of Fig. 3(a). In Fig. 4 we show plots of p_R versus χ for the 2D model of HOCl with the HO bond held fixed at its equilibrium displacement. Comparing

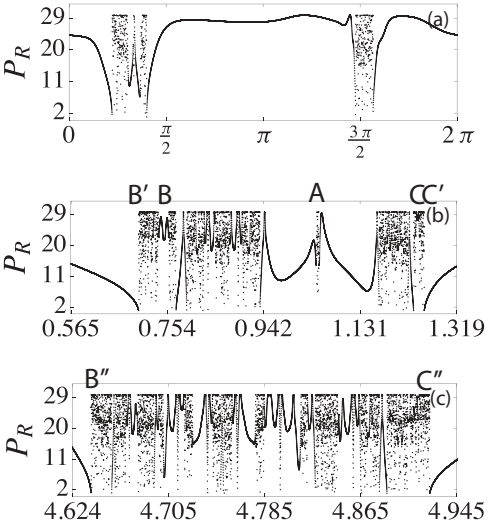

FIG. 4. Scattering dynamics of the 2D Cl-HO system. (a) A plot of p_R versus χ for the case is which the bond length of the HO dimer is held fixed at the equilibrium value $r_{\rm eq} = 1.8389$ d.u., $p_\theta = 5.92$ d.u., and the total energy is fixed at $E = 1.231$ d.u. $= 25\,000$ cm^{-1} (5000 data points for χ). (b) Magnification of left discontinuous region in Fig. 4(a). (c) Magnification of the right discontinuous region in Fig. 4(a). (p_R in dimensionless units and χ in radians.)

Figs. 3(a) and 4(a), we see that the scattering dynamics of the two cases is very similar, although there are also small differences. In both Fig. 3(b) and Fig. 4(b) there are "mirror" points in the discontinuous regions, located directly under the letters B, A, and C. The structures of local regions on either side of these mirror points are approximate mirror images of each other, although the right-hand side is compressed relative to the left-hand side. The large scale similarities between the plots in Figs. 3 and 4 indicate that the 2D model of HOCl is fairly good at reproducing the regions of continuity and discontinuity in the 3D dynamics, as long as the HO vibration is close to its minimum value initially. It therefore appears that a 2D model of HOCl dynamics gives a good approximation to the 3D HOCl dynamics.

Although the plots in Figs. 3 and 4 are very similar, it is clear that small parts of the intervals of continuity in the 2D case contain singular points and become discontinuous in the 3D case. This is seen most clearly when comparing the mirror points B and A in Figs. 3(b) and 4(b), respectively. These mirrorlike structures repeat and can be found embedded locally in these plots as one goes to ever finer scales in the phase space, so there appears to be a fractal structure embedded in the phase space. Using the "box-counting" technique, we have computed the fractal dimension of the intervals of discontinuity that appear to the left- and right-hand sides of Figs. 3(a) and 4(a). For the interval of discontinuity on the left [enlarged in Figs. 3(b) and 4(b)], we find that the intervals of discontinuity for 3D have a fractal dimension of 0.88, while the intervals of discontinuity for 2D have a fractal dimension of 0.80. For the interval of discontinuity on the right [enlarged in Figs. 3(c) and 4(c)], we find that the intervals of discontinuity for 3D have fractal dimension of 0.91, while the intervals of discontinuity for 2D have a fractal dimension of 0.86.

In Fig. 5, we show the time it takes for Cl to leave the asymptotic region at $R = 12$ d.u., interact with HO, and finally return to the asymptotic region at $R = 12$ d.u. for a range of values of initial phase χ in the neighborhood of the mirror point at B. Note that Fig. 5 shows the running times τ for Cl [time for Cl to "run" from its initial position at $R = 12$ d.u., interact with HO (delay time), and then "run" back to its initial position]. The "running time" for a free particle to travel a distance $2R$ is

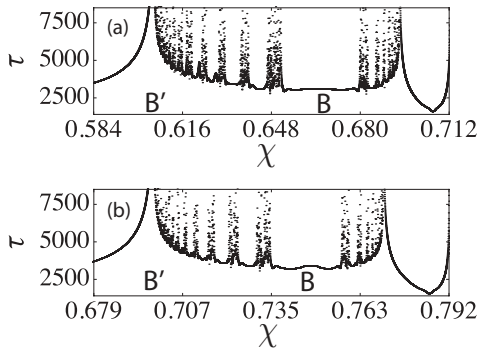

FIG. 5. Running time plots for values of χ in the neighborhood of the mirror point B. Note that these plots contain the time for Cl to travel from $R = 12$ d.u. to the reaction region, then interact with HO and return to $R = 12$ d.u. (a) 3D molecule. (b) 2D molecule. (τ in dimensionless units and χ in radians.)

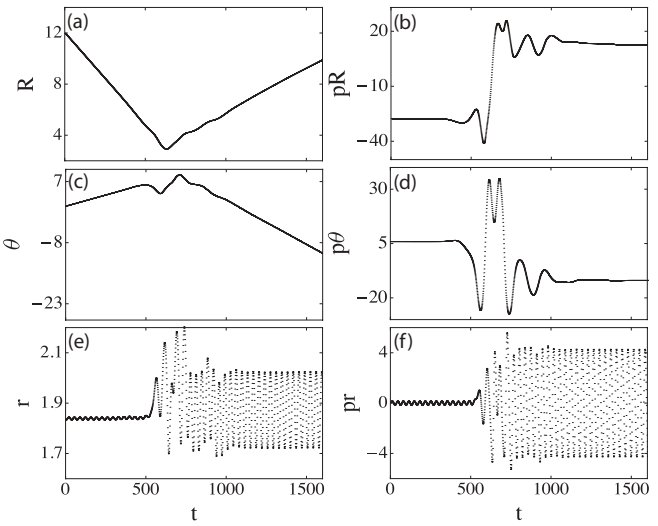

FIG. 6. The scattering dynamics of a single trajectory for $0 \leqslant t \leqslant 1600$, for initial conditions $E = 1.231$ d.u., $\psi = \pi$, and $\chi = 0.967613$. (a) $R(t)$ versus t. (b) $p_R(t)$ versus t. (c) $\theta(t)$ versus t. (d) $p_\theta(t)$ versus t. (e) $r(t)$ versus t. (f) $p_r(t)$ versus t. (p_R, p_θ, p_r, R, r, and t in dimensionless units and θ in radians.)

approximately 3000 d.u. The running time for the 3D case for $\psi = \pi$ and 0.584 d.u. $\leqslant \chi \leqslant 0.712$ d.u. is shown in Fig. 5(a). In Fig. 5(b) we show the running time for the 2D case for the interval 0.679 d.u. $\leqslant \chi \leqslant 0.792$ d.u. (The 3D plot are shifted in χ, relative to the 2D plot, because a small amount of initial energy is shifted from the Cl angular momentum to the HO vibration in the 3D case.) These plots are again very similar, and they show the same fractal structure as the corresponding plots for p_R versus χ. However, the running time plots do have some differences which show that the HO vibration can become involved in the scattering process, even if it has very little energy initially.

It is interesting to compare trajectories from the regions of continuity and discontinuity for the 3D case. In Fig. 6, we show collision dynamics of a single trajectory taken from the region of continuity near the dominant mirror point A in Fig. 3(b). Figures 6(a) and 6(b) show R and p_R versus t, Figs. 6(c) and 6(d) show θ and p_θ versus t, and Figs. 6(e) and 6(f) show r and p_r versus t. The collision takes a very short time. The Cl atom bounces off of HO and is scattered back into the asymptotic region, after having given some of its incident energy to the rotation and vibration modes of HO. The direction of rotation of HO is reversed and the vibration energy of HO is increased by the collision. The time between entering and leaving the collision is approximately $\Delta t_{\text{coll}} = 600$ d.u.

In Fig. 7, we show the collision dynamics of a single trajectory taken from the region of discontinuity around the main mirror point A in Fig. 3(b). For this case, the Cl atom remains in the reaction region for a very long time before it is ejected back into the asymptotic region. For this trajectory, the time between entering and leaving the reaction region is approximately $\Delta t_{\text{coll}} = 1\,015\,800$ d.u. Figures 7(a) and 7(b) show the behavior of R versus t as the Cl enters and leaves, respectively, the reaction region. Similarly, Figs. 7(c) and 7(d) show plots of θ versus t, and Figs. 7(e) and 7(f) show plots of r versus t, as Cl enters and leaves, respectively, the reaction

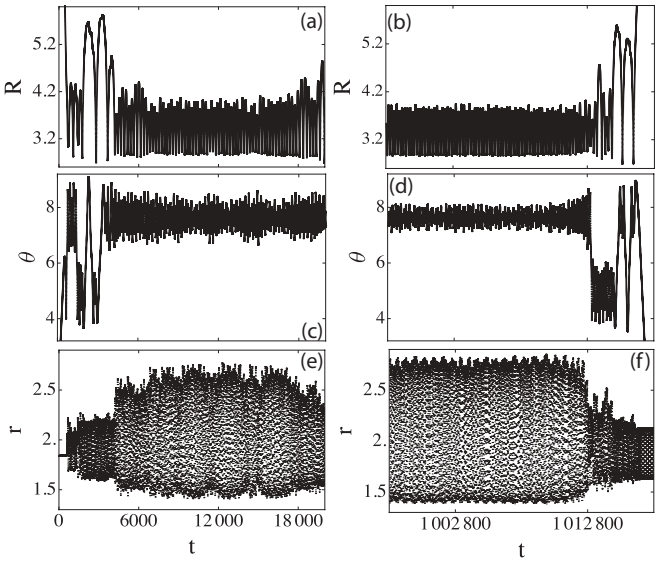

FIG. 7. The scattering dynamics of a single trajectory as it enters the reaction region ($0 \leqslant t \leqslant 20\,000$ d.u.) and as it leaves the reaction region ($997\,800 \leqslant t \leqslant 1\,017\,800$ d.u.), for initial conditions $E = 1.231$ d.u., $\psi = \pi$, and $\chi = 0.994052$. (a) $R(t)$ versus t (entering). (b) $R(t)$ versus t (leaving). (c) $\theta(t)$ versus t (entering). (d) $\theta(t)$ versus t (leaving). (e) $r(t)$ versus t (entering). (f) $r(t)$ versus t (leaving). (R, r, and t in dimensionless units and θ in radians.)

region. The HO-Cl complex appears to be caught up in an oscillatory motion during the entire time that the Cl atom is in the reaction region. Plots of p_R, p_θ, and p_r versus time show variations in oscillation amplitude similar to the plots for $R(t)$, $\theta(t)$, and $r(t)$, respectively, in Fig. 7. In Figs. 8(a), 8(b), and 8(c), we show the power spectra of $R(t)$, $\theta(t)$, and $r(t)$ taken for the interval of time 7000 d.u. $\leqslant t \leqslant$ 17 000 d.u. while Cl is in the reaction region. In all three cases, there are two distinct peaks embedded in a broadened background, indicting that the Cl is likely caught in the neighborhood of an unstable periodic orbit embedded in a chaotic sea associated with the fractal structure. The power spectra for $p_R(t)$, $p_\theta(t)$, and $p_r(t)$ are the same as those shown in Figs. 8(a), 8(b), and 8(c), respectively. Note that the frequencies of the highest peaks is in the ratio 3:5:15, a further indication that the motion of the HO-Cl system is dominated by a periodic orbit of the 3D system.

V. MORE GENERAL INITIAL CONDITIONS

We next examine how the scattering process changes as we vary the division of the initial HO energy between the rotation and vibration degrees of freedom. We fix the total energy at $E_{\rm tot} = 1.231$ d.u. $= 25\,000$ cm^{-1} and the sum of the initial rotational and vibrational energies of HO at value $E_{\rm HO} = 0.1969$ d.u. $= 4000$ cm^{-1}. Thus, the initial value of p_R is held fixed but the incident Cl can have a range of angular momenta, depending on the initial value of p_θ (in order to keep the total angular momentum of the system fixed at zero). In Figs. 9 and 10, we show the result of varying the fraction of the energy $E_{\rm HO}$ that initially goes to rotation and to vibration of the HO dimer. In Fig. 9, we show scattering dynamics when $p_\theta = 5.92$ d.u. and vibration has amplitude in the range

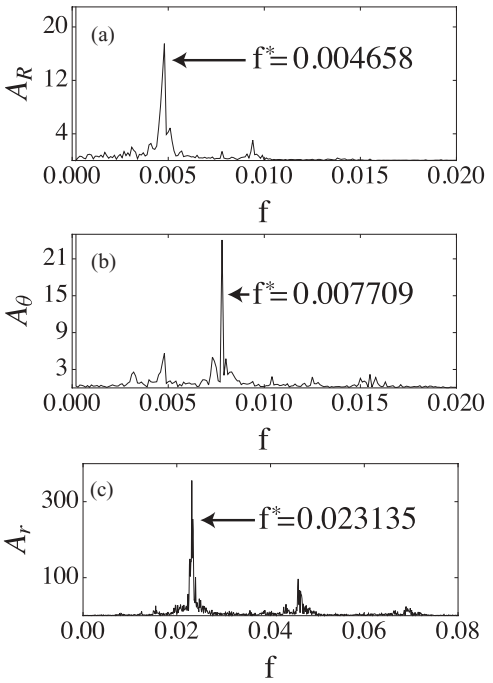

FIG. 8. Amplitudes $A(f)$ of the Fourier transform of the time series in Fig. 7, taken during the time interval 7000 d.u. $\leqslant t \leqslant$ 17 000 d.u., where f is the frequency. (a) $A_R(f)$ versus f taken from time series $R(t)$ versus t. The highest peak is at $f^* = 0.004658$ d.u. (b) $A_\theta(f)$ versus f taken from time series $\theta(t)$ versus t. The highest peak is at $f^* = 0.007709$ d.u. (c) (a) $A_r(f)$ versus f taken from time series $r(t)$ versus t. The highest peak is at $f^* = 0.023134$ d.u. Note that the frequencies of the highest peaks are approximately commensurate with frequency ratios 3:5:15. (A_R, A_r, A_θ, and f in dimensionless units.)

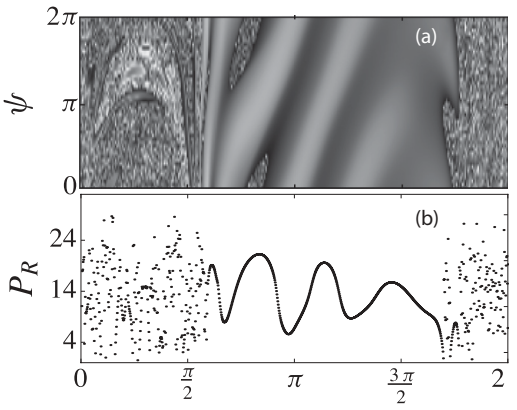

FIG. 9. The total energy is fixed at $E = 1.231$ d.u. $=$ 25 000 cm^{-1}. The energy of the incident chlorine atom is fixed at $E_{\rm Cl} = 1.034$ d.u. $= 21\,000$ cm^{-1}. The remaining $E_{\rm HO} = 0.1969$ d.u. $= 4000$ cm^{-1} is distributed between rotation and vibration of HO so $p_\theta = 5.92$ d.u. and vibration has amplitude in the range 1.622 d.u. $\leqslant r \leqslant 2.134$ d.u. (a) Contour plot of scattered values of p_R as a function of ψ and χ. (b) A plot of scattered values of p_R as a function of χ for $\psi = \pi$. The grayscale in (a) ranges from 0 to 32, with 32 the lightest shade. (p_R in dimensionless units and χ in radians.)

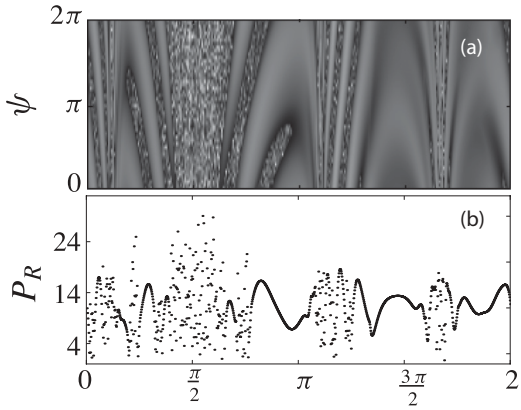

FIG. 10. The total energy is fixed at $E = 1.231$ d.u. $= 25\,000$ cm^{-1}. The energy of the incident chlorine atom is fixed at $E_{\rm Cl} = 1.034$ d.u. $= 21\,000$ cm^{-1}. The remaining $E_{\rm HO} = 0.1969$ d.u. $= 4000$ cm^{-1} is distributed between rotation and vibration of HO so $p_\theta = 0.92$ d.u. and vibration has amplitude in the range 1.599 d.u. $\leqslant r \leqslant$ 2.159 d.u. (a) Contour plot of scattered values of p_R as a function of ψ and χ. (b) A plot of scattered values of p_R as a function of χ for $\psi = \pi$. The grayscale in (a) ranges from 0 to 32, with 32 the lightest shade. (p_R in dimensionless units and χ in radians.)

1.622 d.u. $\leqslant r \leqslant$ 2.134 d.u. The fractal regions have expanded significantly but are still disconnected. Finally, in Fig. 10, we show scattering dynamics when $p_\theta = 0.92$ d.u. and vibration has amplitude in the range 1.599 d.u. $\leqslant r \leqslant$ 2.159 d.u., so the initial energy of HO is almost entirely vibrational. The regions of discontinuity now cover a significant portion of the initial conditions and have a clear dependence on the initial phase of the HO vibration. It is clear from Figs. 9(a) and 10(a) that the scattering dynamics is no longer even approximately independent of ψ as was the case in Fig. 2. As the initial HO vibrational energy increases, the 2D model ceases to be a good approximation of the full 3D dynamics.

VI. CONCLUSIONS

The qualitative behavior of the scattering dynamics of the HOCl molecule, just above dissociation, depends critically on the initial excitation energy of the HO dimer. If the dimer is initially close to its ground state, the scattering dynamics has only small regions of initial conditions that show fractal behavior and the scattering dynamics can be well described by the 2D model. If the HO dimer is initially in a fairly high excited state, a large portion of initial conditions show fractal behavior and the scattering functions show a clear dependence on the initial phase of the HO vibration. In this case, it would appear that the scattering dynamics can no longer be approximated by the 2D model.

The vibrational motion of small molecules, such as HOCl, provides a laboratory for studying the quantum-classical correspondence (QCC) in coupled nonlinear oscillator systems. In a previous paper [17], we studied the QCC using the 2D model of the HOCl molecule. We found that bound states in the quantum system lie primarily on classical periodic orbits, while quasibound states are supported by unstable classical periodic orbits in the continuum. We expect that, in regimes where HO vibration begins to participate in the scattering process, new classes of long-lived quasibound states will be supported by unstable periodic orbits such as those found in Fig. 8. Studies of quasibound state formation, when the HO vibration has significant excitation energy, will require an analysis of the full 3D model of the HOCL molecule.

ACKNOWLEDGMENTS

The authors (Lin, Barr, and Reichl) wish to thank the Robert A. Welch Foundation (Grant No. F-1051) for support of this work. Author Jung wishes to thank CONACyT (Grant No. 79988) and DGAPA (Grant No. IN110110) for support of this work. The authors also thank Kyungsun Na for useful discussions.

[1] C. Jung and H. J. Scholz, J. Phys. A **20**, 3607 (1987); **21**, 2301 (1988).
[2] B. Rückerl and C. Jung, J. Phys. A **27**, 55 (1994).
[3] The collection of articles in *Chaos* (Volume 3, number 4) give an overview of early developments on chaotic scattering.
[4] A. Emmanouilidou, C. Jung, and L. E. Reichl, Phys. Rev. E **68**, 046207 (2003).
[5] C. Jung and A. Emmanouilidou, Chaos **15**, 023101 (2005).
[6] A. Emmanouilidou and C. Jung, Phys. Rev. E **73**, 016219 (2006).
[7] A. M. Barr, K. Na, L. E. Reichl, and C. Jung, Phys. Rev. E **79**, 026215 (2009).
[8] Yi-Der Lin, A. M. Barr, K. Na, and L. E. Reichl, Phys. Rev. E **83**, 056217 (2011).
[9] S. Wiggins, *Normally Hyperbolic Invariant Manifolds in Dynamical Systems* (Springer-Verlag, Berlin, 1994).
[10] C. Jung, O. Merlo, T. H. Seligman, and W. P. K. Zapfe, New J. Phys. **12**, 103021 (2010).
[11] H. Waalkens, R. Schubert, and S. Wiggins, Nonlinearty **21**, R1 (2008).
[12] H. Waalkens and S. Wiggins, Reg. Chao. Dyn. **15**, 1 (2010).
[13] Z. Kovacs and L. Wiesenfeld, Phys. Rev. E **63**, 056207 (2001).
[14] J. Weiss, J. Hauschildt, S. Yu. Grebenshchikov, R. Duren, R. Schinke, J. Koput, S. Stamatiadis, and S. C. Farantos, J. Chem. Phys. **112**, 77 (2000).
[15] We thank R. Schinke for providing access to the PES used in this work.
[16] M. Joyeux, D. Sugny, M. Lombardi, R. Jost, R. Schinke, S. Skokov, and J. Bowman, J. Chem. Phys. **113**, 9610 (2000).
[17] A. M. Barr, K. Na, and L. E. Reichl, Phys. Rev. A **83**, 062510 (2011).